CIRCULATION CONTROL OVER A CIRCULAR CYLINDER BY A SPANWISE ARRAY OF 3D COANDA WALL JETS

Nathan Rackers, Michael DeSalvo, Bojan Vukasinovic and Ari Glezer
Georgia Institute of Technology, Atlanta GA USA

Abstract

Aerodynamic loads engendered by circulation control on a rotorcraft cylinder boom have been used to effect counter torque to replace the conventional tail rotor in NOTAR configurations. These loads that have been realized by the Coanda effect of a 2-D steady wall jet in the rotor downwash, diminish with changes in the direction of the cross flow in sideward and forward flight and are typically augmented by an additional jet thruster. The present wind tunnel investigations explore the utility of segmented Coanda actuation on a circular cylinder model for generating streamwise and cross-stream loads that are insensitive to the direction of the cross flow using spanwise arrays of fluidically oscillating wall jets with specific emphasis on the interaction of the control jets with the cross flow and their effects on the near wake. It is shown that the 3-D jets lead to significant lift increments coupled with increments or decrements in drag. The effects of the 3-D wall jets on separation in adverse pressure gradient over the cylinder's curved surface are investigated using stereo PIV measurements revealing structural features of induced streamwise vorticity concentrations that alter the spanwise interactions with the cross flow. Three-dimensional features of interactions between adjacent jets, entrainment, and vorticity transport are assessed using POD analysis of the instantaneous PIV data.

I. INTRODUCTION

Single rotor helicopters have typically employed a conventional tail rotor to produce the counter torque needed for operation (Sikorsky 1942). However, the tail rotor poses operational disadvantages including mechanical complexity and weight, power loss, added noise, risk of loss of directional control by striking structures, and danger to ground crews (Klemin 1948). Early endeavors to replace the tail rotor focused on the use of the thrust of integrated exhaust air jets for direct control of the torque (e.g. McDaniel 1961).

As an alternative to the tail rotor, the NOTAR ("No Tail Rotor") system was tested on an OH-6A helicopter in the 1970s (Hanvey 1982; Sampatacos et al. 1983; Logan and Kumar 1986). The system produces counter torque by leveraging the Coanda effect resulting from interaction of the main rotor downwash with a nominally two-dimensional wall jet issuing tangentially on a segment of the tail boom. To improve yaw control authority (particularly in forward flight), the wall-jet is augmented with a vectored jet nozzle at the end of the tail boom and a vertical tail. In hovering flight, counter torque is generated primarily by circulation control over the tail boom, while a smaller contribution comes from the vectored tail boom jet with negligible contribution from the vertical tail. Circulation control becomes less effective in rearward and sideward flight, requiring larger thrust from the tail boom jet. In forward flight, yawing moment is provided primarily by the vertical tail and the tail boom jet. Flight tests (Hanvey 1982) demonstrated that the NOTAR system leads to improved hover

stability and reduced noise and vibration, finding the overall concept to be flightworthy, while identifying "unique lateral-directional flying qualities problems at high speed can be eliminated through design modifications." More recently, Luo et al. (2000) assessed the aerodynamic characteristics of a NOTAR helicopter tail boom in a wind tunnel test, finding that the effectiveness of the circulation control component of the system was improved by ~15% by using two jet slots on the same side of the tail boom. Dionisio and Nurick (2001) performed wind tunnel tests of a circular cylinder in a cross flow with two wall jets and assessed the relative contributions to lift and drag of the free stream flow and the wall jets. In a related work, Nurick (2001) tested a circular cylindrical tail boom (terminating in a flat circular surface) in the wake of a rotor and developed a method for estimating the torque of the tail boom using results from two-dimensional wind tunnel data.

The Coanda effect exhibited in the NOTAR system has been the subject of numerous earlier investigations. The evolution of an isolated 2-D turbulent wall jet issuing tangentially over the surface of a cylinder in the absence of a cross flow was first analyzed by in a seminal paper by Newman (1961) who characterized the deflection of the jet along the surface owing to the Coanda effect including the changes in distribution of its cross stream velocity and the surface pressure and the separation of the jet from the surface. Newman also compared wall jets around the cylinder to similar jets along a flat plane and an inclined plane**.** In an experimental investigation, Neuendorf and Wygnanski (1999) characterized the evolution of a wall jet over a circular cylinder, identifying the conditions under which separation occurs compared to a flat plane wall jet. Subsequently, Neuendorf et al. (2004) characterized the streamwise vortices within the turbulent wall jet that are formed on the convex surface due to a centrifugal instability and identified the presence of counter-rotating vortex pairs that migrate along the cylinder axis and were believed to affect separation of the jet from the surface.

In the presence of a cross flow, the Coanda effect over a circular cylinder becomes more prominent, with the flow becoming attached across a larger streamwise extent on one side of the cylinder, resulting in asymmetric flow between the upper and lower sides and a large force normal to the cross flow that is accompanied by changes in the azimuthal position of the front and rear stagnation points and circumferential circulation. Lockwood (1960) reported that a wall jet having momentum coefficient $C_\mu = 0.15$ leads to a normal force of $C_N = 3$, and that larger forces can be realized using multiple tangential jets at successive azimuthal positions. In another remarkable work, Dunham (1968) developed a model based on boundary layer theory and potential flow formulation to estimate the location of separation for a given free stream Re, C_μ, slot width and azimuthal position, from which the resulting C_N was estimated with good agreement with prior experiments**.** In a similar comparison between experiments and a model based on potential flow and boundary layer theory, Levinsky and Yeh (1972) showed that for a given C_μ, C_N is influenced by the jet azimuthal position θ, with maximum C_N for $\theta \sim 110°$. The effect of the wall jet blowing on the drag of the cylinder C_D was studied by Oh and Roberts (1989) who used a discrete vortex model to show up to 4-fold reduction in drag at $C_\mu = 0.1$. The effects of jet position θ and slot width were investigated by Williams and Cummings (1996, $Re = 1.3 \cdot 10^5$) who showed that jets located immediately upstream of separation were most effective at increasing C_N, and that reduction of the slot width enabled the same C_N to be achieved with reduced mass flow. In a combined set of experiments ($Re = 1.1 \cdot 10^5$ and $1.7 \cdot 10^5$) and RANS numerical simulations, Runge et al. (2015) characterized the pressure distributions and corresponding C_N and C_D on the cylinder, finding good agreement between experiments and simulations. Streamlines from the simulations clearly show the flow asymmetry

relative to the direction of the cross flow and the changes in the locations of the front and rear stagnation points. The aerodynamic effects of an *unsteady*, time-periodic 2-D wall jet over a circular cylinder ($Re = 1.9 \cdot 10^5$) were investigated by Ghee and Leishman (1992), who found that for reduced frequencies $k \leq 0.2$, the mean C_N increased ~20%-50% compared to steady actuation at the same C_μ, with a slight reduction in C_D.

The Coanda effect has also been used extensively for circulation control on aircraft wings, e.g. Nichols and Englar (1980) and Englar et al. (2000, 2006), who demonstrated how jet blowing over a wing with a rounded trailing edge ($r = 0.036c$) can increase lift to $C_L \sim 8$-9 at low angles of attack, far exceeding the lift capability of conventional airfoils with multiple-slotted flaps. Loth and Boasson (1984) used circulation control to improve the takeoff and landing performance of an A-6 fighter aircraft and showed that optimization of the control jet characteristics could enhance its effectiveness for improving high lift performance. In wind tunnel tests of a circulation control wing with trailing edge radius $r = 0.02c$, Jones and Englar (2003) showed that by using pulsed blowing through a full-span slot, the mass flow needed to achieve a given C_L was reduced by about 50%. While the earlier studies of the Coanda effect used primarily 2-D wall jets, recent circulation control investigations by Vukasinovic et al. (2023) demonstrated the utility of arrays of unsteady, 3-D fluidically-oscillating wall jets on a 2-D wing with a cylindrical trailing edge. These authors showed that while both 2-D and 3-D circulation control led to lift increments of up to $\Delta C_L \sim 2$ at $C_\mu \sim 0.1$, the drag increment in the presence of 2-D actuation was significantly higher (up to 60%) than with 3-D actuation.

The present wind tunnel investigations explore segmented circulation control on a circular cylinder model using the Coanda effect of 3-D oscillating wall jets with specific emphasis on the induced streamwise and cross-stream aerodynamic loads and the dynamics of the structure of interactions between the control jets and the cross flow and their effects on the near wake. The experimental setup is described in §II. The effects on aerodynamic loads due to actuation in the presence of various surface trip configurations are discussed in §III, and details of the flow physics of the interaction between the jet array and the cross flow are discussed in §IV.

II. EXPERIMENTAL DESCRIPTION

A 2-D circular cylinder wind tunnel model of radius $D = 152$ mm and span $S = 885$ mm (Figure 1a) comprising five spanwise segments of equal length, each with an integral spanwise array of fluidic actuators for circulation control, is used in the present experiments. The model is mounted to two 6-component load cells on either side of the wind tunnel's square test section (91.4 cm on the side) having a maximum speed of 35 m/s. The azimuthal coordinate over the cylinder surface

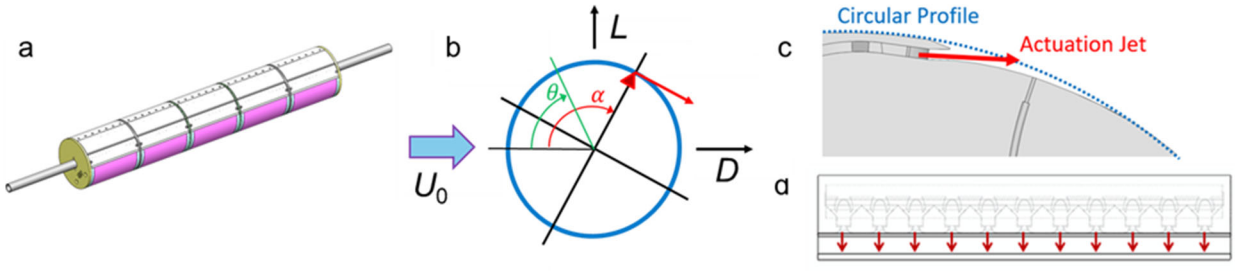

Figure 1. *(a) Spanwise-segmented circular cylinder wind tunnel model, (b) Schematic of model cross section, (c) Actuator jet exit and circular profile of model, (d) Array of fluidically oscillating jets.*

θ and azimuthal position of the jet array α (adjusted by rotating the model about the centerline) are each measured relative to the front stagnation point in the absence of jet actuation, and vertical and horizontal loads L and D model the rotorcraft tail boom side force and download, respectively (Figure 1b). The present experiments are performed primarily at a free stream speed of U_0 = 25 m/s ($Re_c = 2.1 \cdot 10^5$).

The model segments each consist of a cylindrical aluminum shell integrated with an actuation segment fabricated using stereolithography. Each actuation segment consists of a spanwise array of surface-tangential fluidically oscillating actuation jets (Figure 1c), a separable plenum, and a spanwise array of static pressure ports. The model is equipped with azimuthal disc inserts, each containing 54 static pressure ports, for measuring the azimuthal pressure distribution around the cylinder at different spanwise locations between the primary segments. The center spar is hollow and supplies air through pneumatic connections to the plenum of each spanwise segment. The jet array in each spanwise segment consists of discrete wall jets oscillating spanwise with a nominal frequency of 3-4 kHz that are spaced every 24.8 mm with orifices of height 1.52 mm and width 1.26 mm (Figure 1d).

The flow at the exit plane of each actuator jet module was surveyed using a total pressure probe mounted on a traverse to assess the spanwise variation of the jet velocity in the absence of cross flow 0.087D downstream of the jet exit plane (the velocity was inferred from the estimated the dynamic pressure) as shown in Figure 2a. These data show that each jet spans about 0.12D and that the spanwise variations in peak velocity are within 10% owing to slight variations in the SLA tolerance.

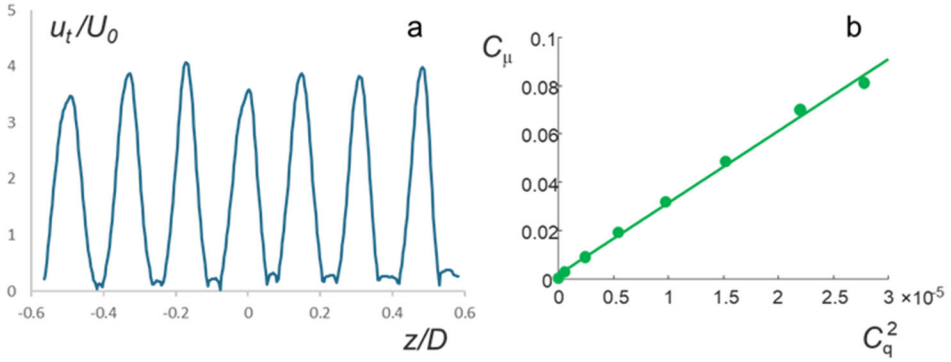

Figure 2. *(a) Spanwise variation of actuator streamwise velocity measured 0.087D downstream from jet exit plane, (b)Variation of C_μ^F with C_q^2.*

The thrust of the actuation jets is characterized using a dimensionless actuation aerodynamic force coefficient: $C_\mu^F = F_{act}/(\frac{1}{2}\rho {U_0}^2 DL)$ that is a variant of the conventional momentum coefficient and is a measure of the magnitude of the resultant aerodynamic force effected by the fluidic actuator array on the aerodynamic platform in which it is integrated in the absence of crossflow. This actuation force coefficient measures, in effect, the magnitude of the actuation force $\boldsymbol{F_{act}}$ that is necessary to alter the cross flow with free stream dynamic pressure $\frac{1}{2}\rho {U_0}^2$ to yield the measured changes in the aerodynamic loads relative to the baseline loads when the actuation is inactive. The aerodynamic force coefficient C_μ^F was be measured directly *in situ* using the load cells. The actuation mass flow rate $\dot{m}_{jet}$ is measured using a thermal mass flow meter, used to compute the mass flow rate coefficient $C_q = \dot{m}_{jet}/(\rho_o U_o L)$. Figure 2b shows that, as expected, and $C_\mu^F \sim (C_q)^2$ (at U_0 = 25 m/s, the maximum C_μ^F was 0.08).

The flow over the leeward side of the cylinder, in the presence and absence of actuation was characterized using stereo particle image velocimetry (sPIV) in seven planes normal to the local surface tangent, yielding three velocity components namely the in-plane radial and spanwise components and the tangential velocity normal to the plane as illustrated in Figure 3. The wake was characterized using measurements in a streamwise-normal plane 0.84*D* downstream of the cylinder' center. The flow is seeded with micron-size fog particles, that are illuminated using a double-pulsed Nd:YAG laser. Image pairs are captured using two 2640 x 2300 pixel CCD cameras downstream of the PIV plane on opposite sides of the wind tunnel. The present measurements form ensembles of 500 instantaneous vector fields where the ensemble-averaged data are used to obtain distributions of velocity, turbulent stresses and in-plane vorticity. Modes of the instantaneous flow fields are computed using Proper Orthogonal Decomposition (POD, e.g. Sirovich 1987, Berkooz et al. 1993), and reconstructions of the instantaneous data using the 30 highest-energy modes (about 1/3 of the total oscillatory energy) are used to assess interactions between the oscillating jet and the cross flow. In addition the separated flow and near wake on the leeward side of the cylinder were characterized using spanwise-normal planar PIV in a set of five overlapping views. Velocity measurements in individual measurement windows are combined to a single composite grid.

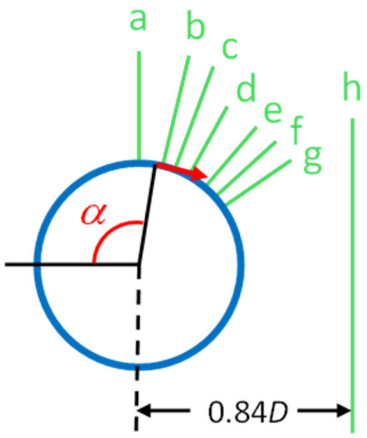

Figure 3. *Stereo-PIV measurement planes normal to local surface tangent: θ = 90°(a), 108°(b), 116°(c), 125° (d), 138° (e), 146° (f), 156° (g). The measurement plane in the near wake is normal to free stream (h) 0.84D downstream of cylinder center.*

III. AERODYNAMIC EFFECTS OF COANDA JET ARRAYS

The pressure distribution over the cylinder ($Re_D = 2.1 \cdot 10^5$) was characterized with the fluidic actuation array at $\alpha = 120^o$ for which lift in the presence of actuation is maximized. However, in the absence of actuation, the azimuthal pressure distribution on the baseline cylinder was asymmetric between the upper and lower surfaces, owing to asymmetric separation in the presence of the actuation jet array that resulted in non-zero lift. This asymmetric

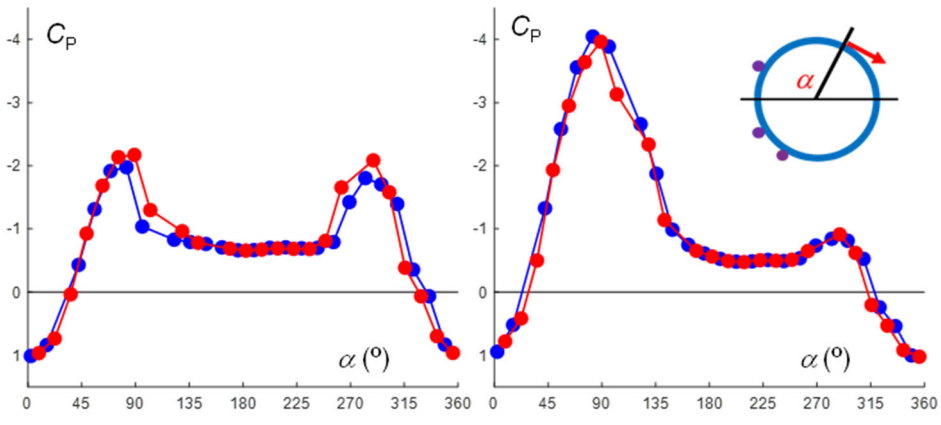

Figure 4. *Azimuthal static pressure distributions (red and blue) at the spanwise edges of the center segment with trips at θ = 30°, 330° and 305°: C_μ^F = 0 (a) and 0.052 (b).*

pressure distribution was nearly eliminated by placing boundary layer trips (0.0026D thick tape) at $\theta = 30°$ and 330° and an additional trip at $\theta = 305°$ to compensate for the presence of the actuation module yielding a nearly-symmetric pressure distribution (Figure 4a). In the presence of actuation ($C_\mu^F = 0.052$, Figure 4b) a strong suction peak forms on the upper surface (up to $C_p = -5$) indicative of the low pressure induced by the Coanda effect of the wall jets that decreases to the level of the base pressure in the wake at $\theta \approx 150°$. It is remarkable that the presence of the actuation leads to a significant reduction in the base pressure of the cylinder ($\Delta C_p \approx 0.2$) accompanied by a weaker suction peak on the bottom surface of the cylinder, indicating an increase in drag. The variation of the lift and drag with C_μ^F are shown in Figures 5a and b, respectively. The lift (Figure 5a) increases nearly monotonically with C_μ^F, with a maximum $C_L = 3.2$ at $C_\mu^F = 0.091$. The drag (Figure 5b) varies minimally with C_μ^F, having values of $C_D \sim 0.54$ for $C_\mu^F < 0.025$ and $C_D \sim 0.65$ for $C_\mu^F > 0.025$. By comparison, a similar experiment by Ghee and Leishman (1992, $Re_D = 1.9 \cdot 10^5$) with tangential blowing from a 2-D slot at $\alpha = 100°$ and trips at $\theta = 60°$ and 300° reported $C_D \approx 0.7$ and nearly zero lift in the absence of actuation, while for $C_\mu^F = 0.07$, $C_L = 2$ and $C_D = 0.5$ were observed, in good agreement with the present measurements.

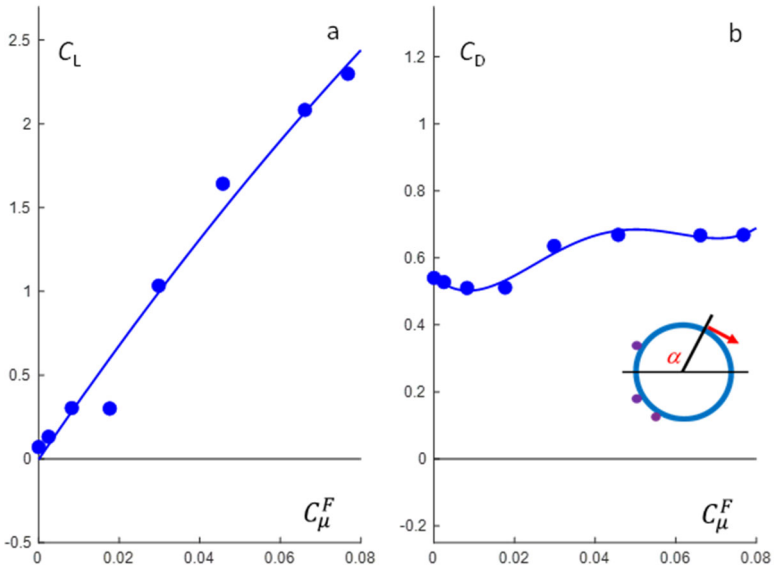

Figure 5. *Variation with C_μ^F of normal load C_L (a) and streamwise load C_D (b) with trips at θ = 30°, 330° and 305°.*

The measurements in Figures 4 and 5 were obtained with surface trips at fixed azimuthal positions. Since the presence of the inactive actuator ports influences flow separation on the leeward side of the cylinder in the absence of actuation, adjustment of the actuator azimuthal position leads to changes in the flow in the absence of actuation. Therefore, to mitigate the effect of the azimuthal position of the inactive actuator on the unactuated flow, spanwise tape trips were installed around the circumference of the cylinder at equally-spaced azimuthal positions 10° apart. Figures 6a and b show the respective variation of C_L and C_D with azimuthal actuator position $40° \le \alpha \le 160°$ for $C_\mu^F = 0$, 0.008, 0.031, 0.068 and 0.077. The variations of the aerodynamic loads with α in the absence of actuation show relatively small variations in drag between $0.5 < C_D < 0.6$, i.e. ~8% of the average value. The drag is comparable to levels for a circular cylinder with a rough surface ($k/D \sim 0.002$) at $Re_D = 2 \cdot 10^5$ (Hoerner 1965) and is similar to levels measured by Shih et al. (1993) on a smooth cylinder at $Re_D \sim 3\text{-}4 \cdot 10^5$ that is associated with transition to turbulence of the surface boundary layer suggesting that the use of the azimuthally-periodic trips reduces somewhat the sensitivity of the unactuated flow to the actuator position by promoting transition to turbulence on the windward side of the model as it is rotated although the variations

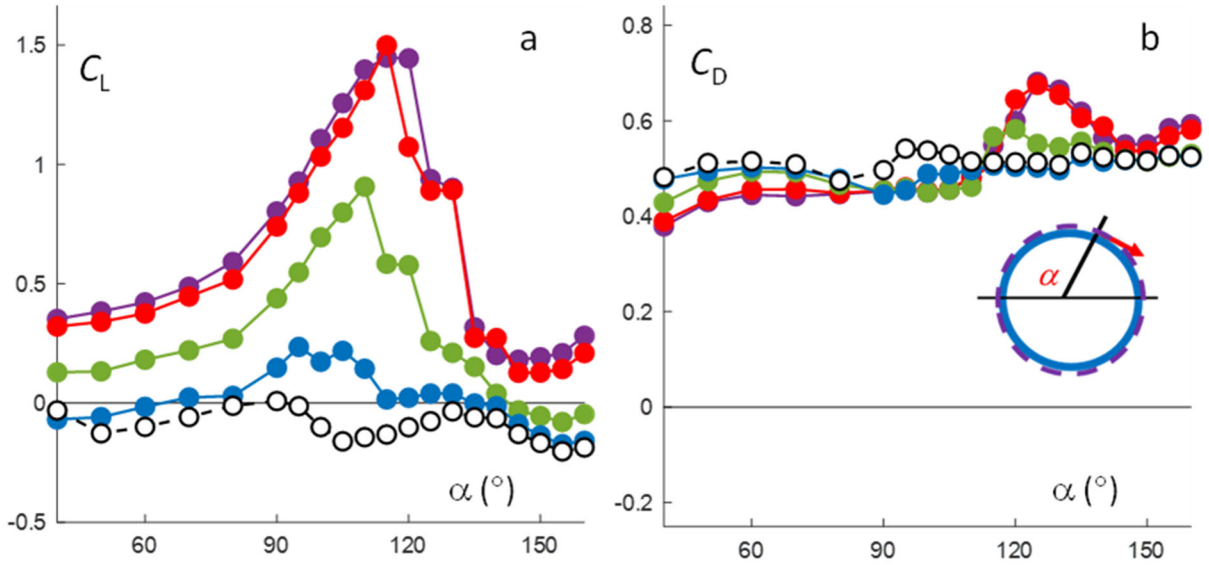

Figure 6. *Variation the normal load C_L (a) and streamwise load C_D (b) with the actuation position α for azimuthally periodic trips and actuation at C_μ^F = 0 (○), 0.6% (●),3.0% (●), 6.7% (●) and 8.7% (●).*

in lift are up to -0.2 (-0.2 < C_L < 0). In the presence of actuation, C_L (Figure 6a) increases monotonically with α for 40° < α < 90° and with C_μ^F, reaching levels of 0.4-0.5 for C_μ^F = 0.087, while the drag (Figure 6b) decreases with increasing C_μ^F from the baseline level (C_D ~ 0.5) to as low as 0.35 at α = 40°. The combination of the lift and drag indicates that the Coanda force vector is inclined upstream when the actuation is applied on the windward side of the cylinder. As the actuation is moved to 90° < α < 110°, the rate of increase of C_L with C_μ^F increases reaching a peak of 1.5 at C_μ = 0.067 and 0.087, indicating that the actuation is more effective in turning the flow with no significant change in C_D. Within 110° ≤ α ≤ 135, the location of separation in the absence of actuation (cf. §IV), the lift increment due to actuation decreases substantially and the actuation leads to increased pressure drag owing to the increase of suction at the base of the cylinder, reaching C_D ~ 0.7 (cf. Figure 4). Moving the actuator to α > 135° leads to lower levels of C_L which remain invariant with α, while drag remains nearly equal to the baseline level (~0.5).

To assess the flow physics without the effects of trips, the model was covered with smooth monolithic skin covering the entire circumference of the cylinder except a 30° segment downstream of the actuator. Figure 7 shows the variation of C_L and C_D with α for C_μ^F = 0, 0.008, 0.031, 0.068, and 0.077. In the absence of the spanwise-periodic trips (cf. Figure 6), the drag varies roughly between two levels of C_D ~ 0.8 for 40° < α < 80° and C_D ~ 1.2 for 110° ≤ α ≤ 160° (except around 105°). The presence of the jet array on the leeward side of the cylinder is not expected to affect the transition and separation of the upper surface boundary layer and the drag is comparable to a smooth cylinder (Hoerner 1965). However, the presence of the jet array on the windward side leads to the boundary layer transition to turbulence on the smooth surface as indicated by the lower drag and the lift that is associated with the resulting asymmetric flow. As noted by Zdravkovich (1990) surface roughness on a circular cylinder can lead to boundary layer transition and drag crisis at a lower Re_D and eliminate some transitional flow regimes. It is noted that in the absence of actuation, C_L decreases from ~0.3 for α ≤ 70° to ~0 for 110° ≤ α ≤ 160°.

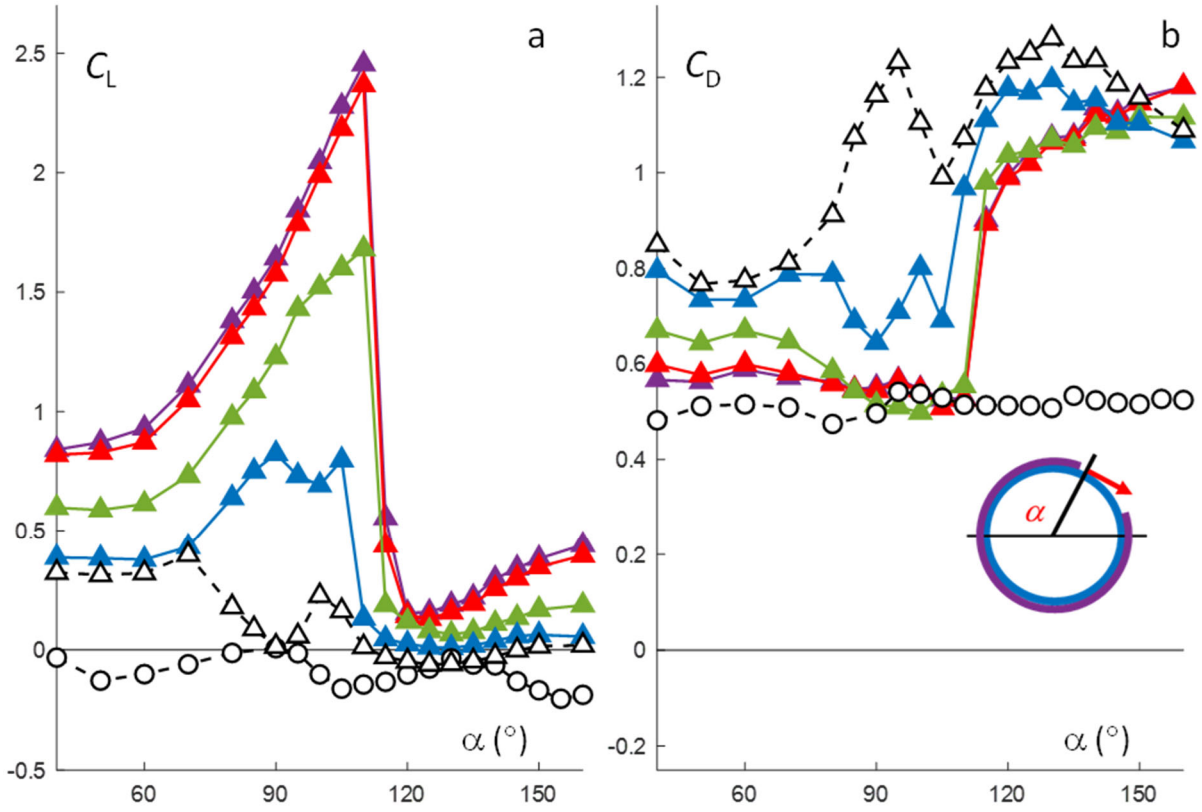

Figure 7. *Variation the normal load C_L (a) and streamwise load C_D (b) with the actuation position α for a smooth cylinder and actuation at: C_μ^F = 0 (Δ), 0.008 (▲), 0.031 (▲), 0.068 (▲) and 0.076 (▲).*

As C_μ^F increases, C_L increases while C_D decreases, indicating that actuation can be used both to generate normal load and simultaneously reduce streamwise load. For $C_\mu^F \geq 0.03$, normal load increases monotonically with α up to $\alpha = 115°$. For $\alpha = 115°$ and $C_\mu^F = 0.076$, the lift reaches a peak of $C_L = 2.5$ that is comparable to the measurements with the fixed trips at $\alpha = 120°$ (cf. Figure 5), while drag is reduced to $C_D \sim 0.5$ from $C_D \sim 1$, suggesting that actuation leads to a reduction in the wake width and does not reduce the cylinder's base pressure. As the actuation is moved to $\alpha > 120°$ it no longer affects the cross flow to the same extent, as is shown by the drastically reduced changes in both C_L and C_D compared to a jet location of $\alpha = 115°$.

It is noteworthy that the lift generated by the fluidically oscillating jets at a given mass flow rate can be an order of magnitude higher than the corresponding lift generated by a 2-D jet. For example, the circular cylinder data of Williams et al. (1996, $Re_D = 1.32\text{x}10^5$, $\alpha = 90°$, $t/D = 0.0025$) shows that at $C_q \sim 0.006$, a 2-D jet produced $C_L < 0.1$ compared to $C_L \sim 1.7$ produced by the present jets at the same C_q.

IV. INTERACTION OF COANDA JET ARRAYS WITH CROSS FLOW

The effects of the actuator array on the boundary layer, separating shear layer, and near wake of the cylinder were characterized using spanwise-normal 2-D PIV measurements over the model surface and in the near wake at the spanwise center ($z = 0$; Figure 8). The model was configured as with the results in in Figure 4, and the jet array was placed at $\alpha = 120°$. In the absence of

actuation (Figure 8a), the flow separates near the jet orifices (θ = 120°) and significant reverse flow is present in the wake. With actuation (C_μ^F = 5.1%; Figure 8b), the Coanda jet interacts with the surrounding flow leading to a substantial increase in downwash that is associated with increased lift (cf. Figure 5c). As shown, the flow near θ = 90° is accelerated from ~1.5U_o to ~2U_o, and an attached boundary layer is formed on the leeward side as far downstream as θ = 160° with a significantly diminished wake domain. The turning of the outer flow towards the actuated side of the cylinder extends into the near wake.

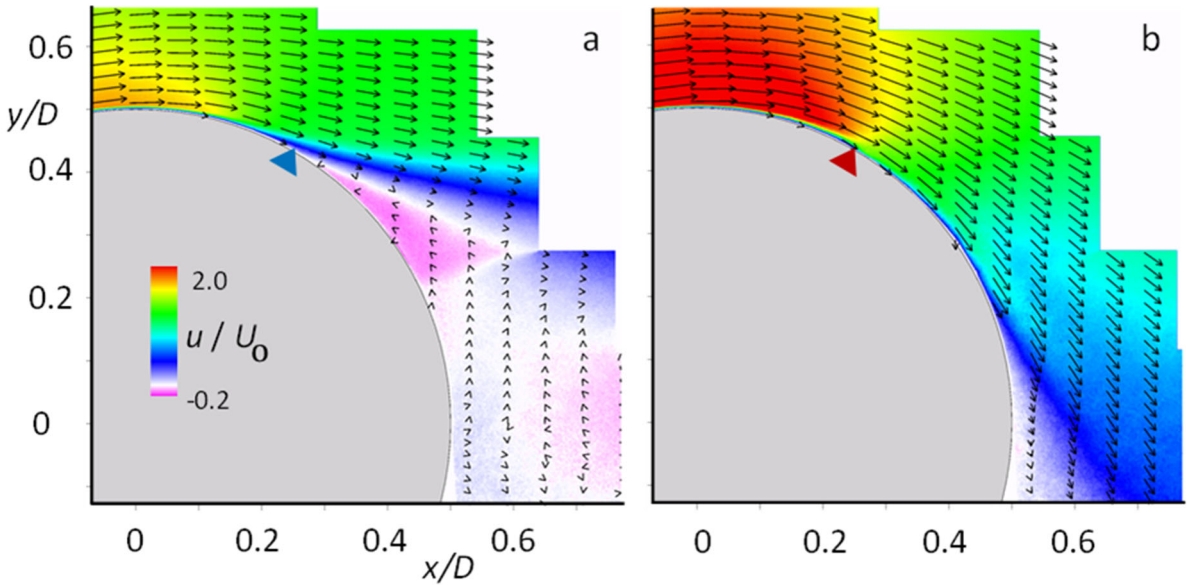

Figure 8. *Time-averaged spanwise-normal flow field around cylinder centerline (z = 0) with streamwise velocity color contours, trips on windward side (cf. Figure 4,5) and jets at α = 120°. C_μ^F = 0 (a), 0.051 (b).*

The interaction of the jets with the cross flow was characterized for a smooth cylinder (cf. Figure 7) using stereo PIV in planes normal to the local surface tangent at θ = 90°, 108°, 116°, 125º, 138º, 146º, and 153º (cf. Figure 3) with the actuator jet array at α = 100°. Additional measurements were taken in a streamwise-normal plane 0.84D downstream of the model center to characterize the near wake.

Time-averaged radial distributions of the azimuthal velocity normal to the local surface at z = 0 are shown in Figure 9 for C_μ^F = 0, 0.008, 0.031, and 0.067, along with a vector showing the magnitude and direction of the total aerodynamic load. In the absence of actuation (C_μ^F = 0; Figure 9a), the maximum streamwise speed at θ = 90° is ~1.5U_0 and the total aerodynamic load is not entirely streamwise but contains some passive lift. As C_μ^F is increased to 0.8% (Figure 9b), the outer flow is turned toward the actuated surface, separation is delayed to θ ~ 128°, and lift is increased (cf. Figure 7a) while reverse flow near the wall downstream of the actuator is diminished, leading to reduced drag (cf. Figure 7b). Increasing the actuation to C_μ^F = 0.031 (Figure 9c) and 0.067 (Figure 9d) results in an increased extent of flow attachment, with the maximum streamwise velocity at θ = 90° increasing to ~2U_0 and separation delayed to θ ~ 138° and 150°, respectively. By comparison, in the presence of the trips (cf. Figure 8), separation is moved to θ ~ 160° with C_μ^F = 0.051 ostensibly due to boundary layer transition upstream of the jets, leading to improved jet effectiveness. For all $C_\mu^F \geq$ 3.1%, the drag decreases to a nominally fixed level C_D ~ 0.55 (cf.

Figure 7b), while lift increases monotonically with C_μ^F, resulting in the total aerodynamic loading becoming predominantly cross-stream.

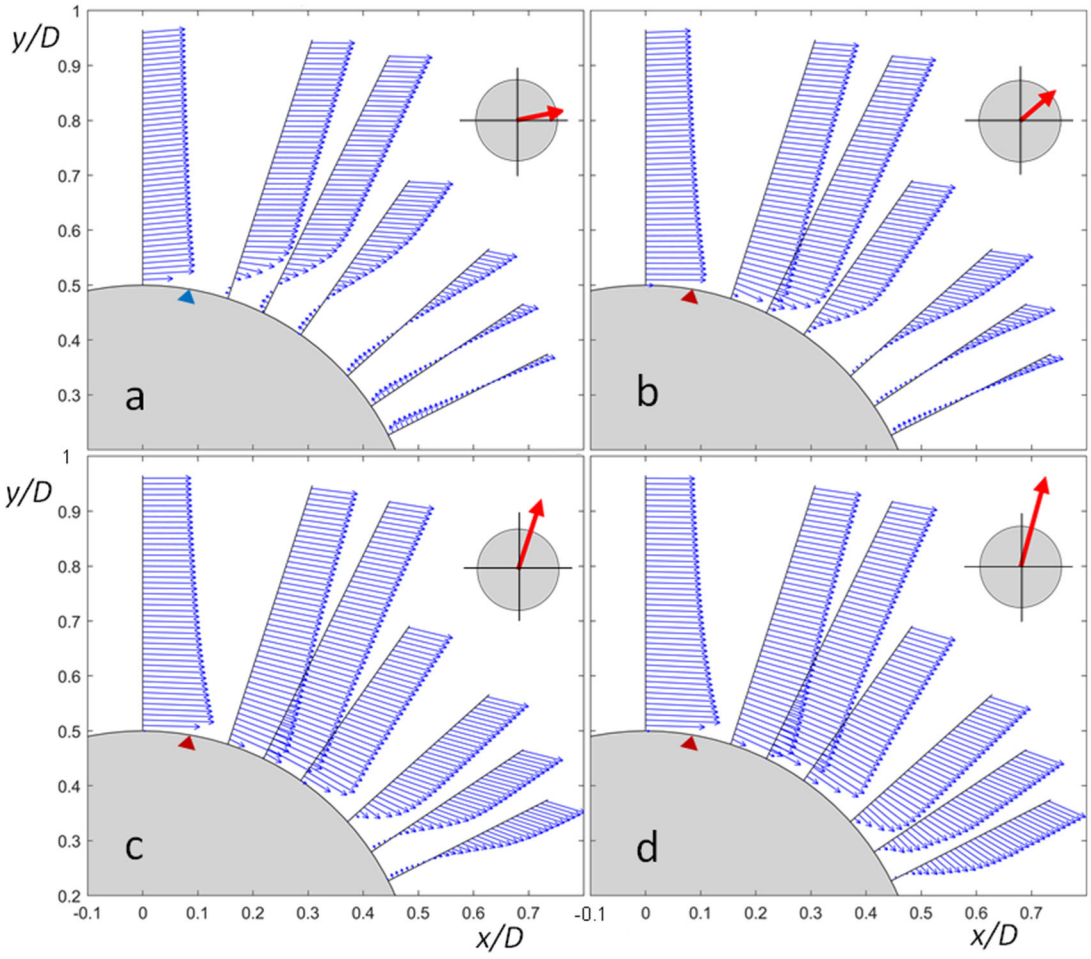

Figure 9. *Time-averaged radial distributions of azimuthal velocity component normal to the local surface at $z = 0$ for smooth cylinder with actuation jets at $\alpha = 100°$: $C_\mu^F = 0$ (a), 0.008 (b), 0.031 (c), and 0.067 (d). The magnitude and direction of total aerodynamic load is marked by red arrows on the right of each image.*

Color raster plots of the time-averaged tangential velocity u_t superposed with in-plane velocity vectors in *r-z* radial planes at $\theta = 108°$, 116° and 136° shown in Figures 10a-f in the absence (a, c, and d) and presence (b, d, and f) of actuation (the radial distance above the surface is denoted h) The radial and spanwise velocity components are u_r and w, respectively, where $u_r > 0$ denotes flow away from the surface). In the absence of actuation ($C_\mu^F = 0$; Figures 10a, c ,e) the flow is nearly spanwise-uniform at all three azimuthal locations and becomes increasingly radially-outward as h increases due to the strong adverse pressure gradient on the leeward side of the cylinder (cf. Figure 4), while separation occurs at $\theta = 108°$ as indicated by the presence of reverse flow adjacent to the wall. In the presence of actuation ($C_\mu^F = 0.031$; Figures 10b, d, f), separation moves downstream to $\theta = 136°$, and is most pronounced near $z/D \sim 0.1$, and the spanwise periodicity imposed by the the actuation jets is evident at all three azimuthal positions. At $\theta = 108°$ in the presence of actuation (Figure 10b) and $h/D = 0.03$, u_t has higher levels above jet centers than between the jets.

However, the spanwise maxima of u_t do not coincide with the jet locations and vary with streamwise distance from the actuators. For example, the maximum of u_t associated with the jet orifice at $z/D = 0.16$ migrates from $z/D = 0.16$ at $\theta = 108°$ (8° downstream of the jets) to $z/D = 0.19$ at $\theta = 136°$ (36° downstream of the jets). It is conjectured that the misalignment between spanwise jet locations and maxima of u_t occurs due to the random phase of the spanwise oscillation of individual jets that results in random interactions with neighboring jets and some differences in jet strength (cf. Figure 2). It should be noted that the time-averaged flow structure is of course significantly different from the instantaneous flow structure that is characterized by chaotic interactions between adjacent fluidically oscillating jets that operate at a random phase.

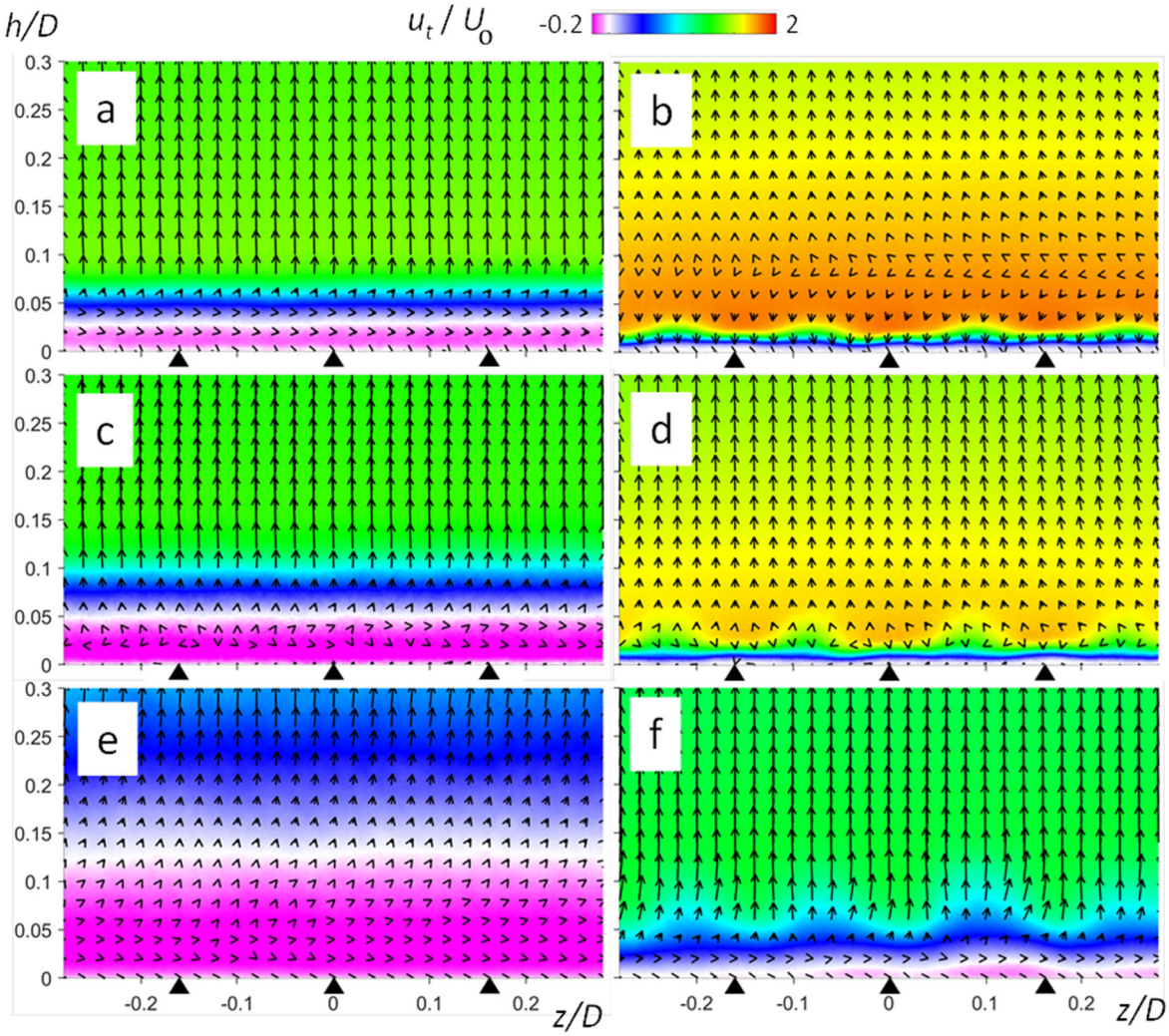

Figure 10. *Time-averaged flow fields normal to local surface tangent (cf. Figure 2) and color contours of tangential velocity for smooth cylinder with jets at a = 100°: θ = 108° (a, b), 116° (c, d) and 136° (e, f).* $C_\mu^F = 0$ *(a,c,e), 3.1% (b,d,f). Triangles denote spanwise positions of jets.*

In the presence of actuation, the time-averaged radial velocity u_r near the wall becomes more negative (oriented toward the wall). For instance, at $\theta = 108°$ (Figure 10b), u_r is negative for $h/D < 0.08$, where u_t has values of up to $1.8U_0$, while at $\theta = 116°$ (Figure 10d), u_r is negative only

for $h/D < 0.03$, and u_t is as large as $1.7U_0$. This suggests that actuation results in higher-momentum fluid from above the wall being drawn toward the surface, and that the effect is strongest near the jet orifice and diminishes with increasing downstream distance from the orifice.

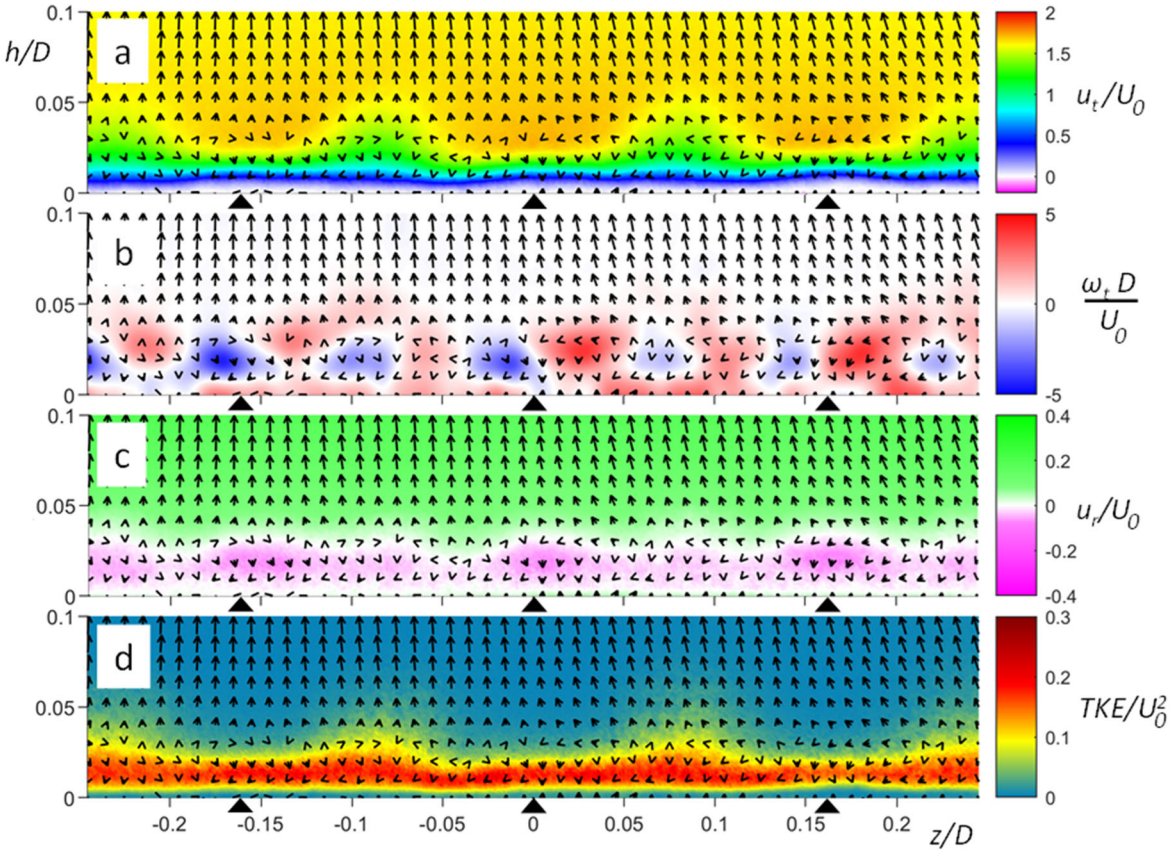

Figure 11. *Time-averaged flow fields normal to local surface tangent at $\theta = 116°$ (cf. Figure 2) for smooth cylinder with jets at $\alpha = 100°$ and $C_\mu^F = 3.1\%$. Color contours of (a) tangential (out-of-plane) velocity, (b) in-plane vorticity, (c) radial velocity, and (d) turbulent kinetic energy. Triangles denote spanwise positions of jets.*

To more clearly elucidate the effect of the jets, Figure 11 shows time-averaged in-plane velocity vectors along with color contours of u_t, in-plane vorticity ω_t, u_r and turbulent kinetic energy (TKE) in the presence of actuation ($\alpha = 100°$, $C_\mu^F = 3.1\%$) at $\theta = 116°$ (cf. Figure 10d). The tangential velocity (Figure 11a) at $h/D = 0.004$ is at a minimum at the spanwise jet centers and has local maxima $0.04D$ to either side, as a result of the fluidically oscillating jets spending more time oriented to the extremes of their oscillation than in the streamwise direction. However, further above the wall (e.g. $h/D = 0.03$), u_t approaches a maximum in domains spanning $\pm 0.04D$ from the jet centers, and a minimum between jet centers. The corresponding in-plane vorticity (Figure 11b), with red and blue denoting clockwise and counterclockwise vorticity, respectively, shows counter-rotating vortex pairs within $0.05D$ of the wall. For each jet, two counter-rotating vortex pairs are present with radially-outward induced flow between the vortices, with the spanwise centers of each pair located $\pm 0.04D$ from the spanwise center of the jet. Along the spanwise center of each jet, opposite vortices from the two pairs interact, with a radially-inward induced flow along the jet centerline. This is shown more clearly in the color contours of radial velocity (Figure 11c) where u_r is more negative along the jet centerlines, and less negative $0.04D$ to either side. Moving radially outward from the wall (where $u_r = 0$) toward $h/D \sim 0.015$, u_r becomes increasingly negative

(radially-inward), before the velocity gradient reverses, leading to positive u_r for $h/D > \sim 0.03$. In accordance with the continuity equation for incompressible flow, neglecting the spanwise velocity component, this indicates that the streamwise velocity is accelerating for $h/D \leq 0.015$, where the effect of the jet is most pronounced, and decelerating for $h/D > 0.015$, where effects associated with the global flow around the cylinder predominate.

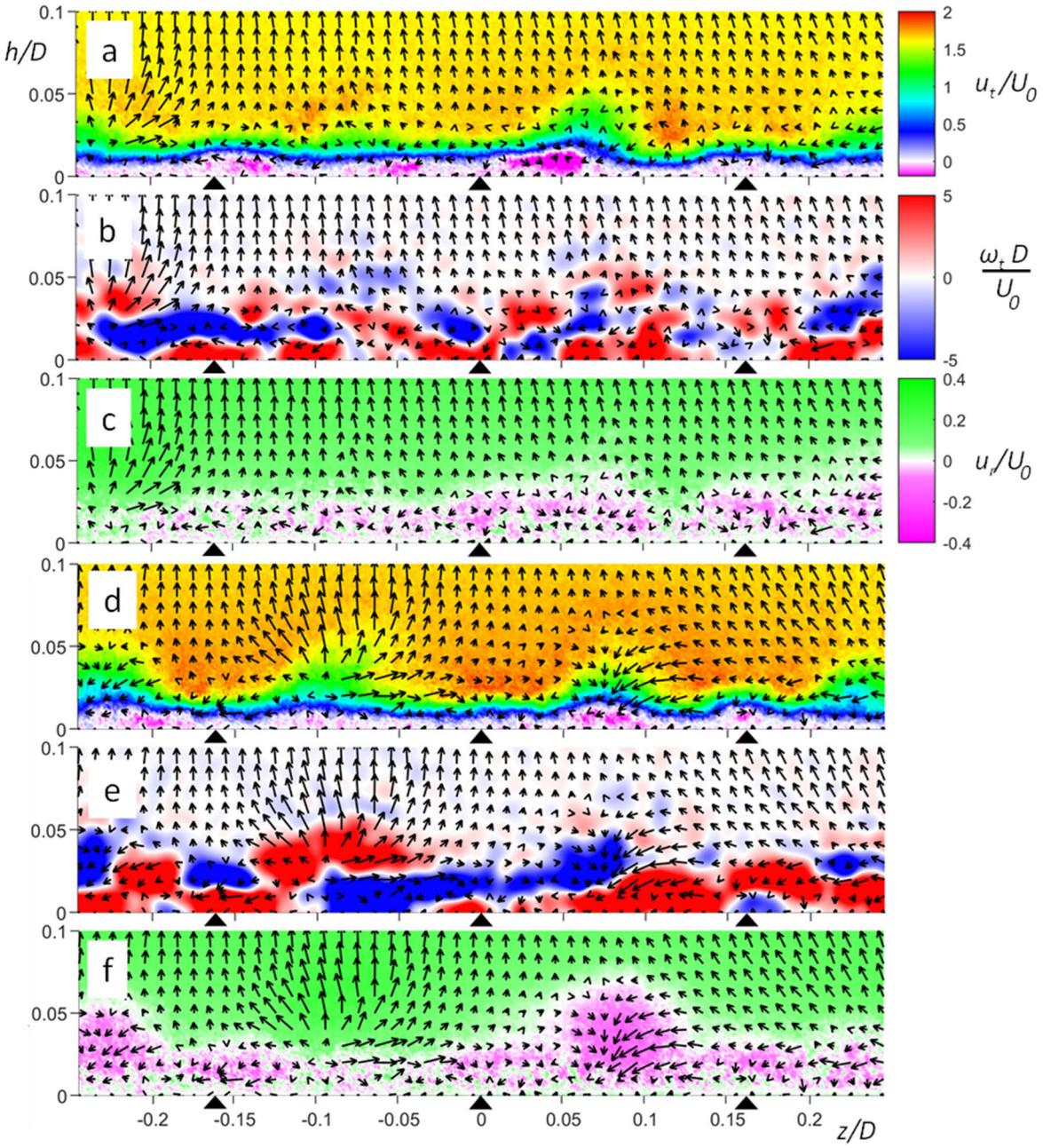

Figure 12. *POD reconstructions of instantaneous flow fields from measurements in Figure 11: Realizations I (a,b,c) and II (d,e,f). Color contours of (a,d) tangential (out-of-plane) velocity, (b,e) in-plane vorticity and (c,f) radial velocity. Triangles denote spanwise positions of jets.*

These effects are explained using the results of Launder and Rodi (1983), who show how the interaction between a surface and a tangentially-oriented 3-D jet (i.e. with limited spanwise extent)

leads to the formation of a counter-rotating streamwise vortex pair with induced flow away from the surface between the vortices, and induced flow toward the surface to either side of the vortex pair, leading to enhanced spreading compared to a conventional jet and fluid transfer between the jet core and the surroundings. As a result, in the presence of a cross flow, higher-momentum fluid from the cross flow is transferred toward the wall. However, because the measurements in Figure 11 are taken using spanwise-oscillating jets, each of which are oriented toward one side or the other for most of the cycle, the mean flow contains *two* streamwise vortex pairs for each jet, each with radially-outward induced flow, corresponding to the two respective orientations of the jet. Between the vortex pairs and the wall, the flow is influenced predominantly by the jets, and therefore the peaks in streamwise velocity occur near the spanwise edges of the jet, where the jet is oriented for most of the cycle. However, above the vortex pairs, the flow is influenced predominantly by the interaction with the cross flow that is characterized by transfer of high-momentum fluid from the cross flow toward the wall, resulting in streamwise velocity maxima above the jet centers spanning an extent far larger than the jet width due to the jet oscillation, and minima between jets. This is supported by the measurements of TKE (Figure 11d) which is highest for $h/D < 0.02$, where effects of the randomly oscillating jets predominate, and nearly zero for $h/D > 0.04$, in the cross flow. For $0.02 \leq h/D \leq 0.04$, TKE is nearly zero above jet centers, where high-momentum fluid is drawn toward the surface, and increases between jet centers, where the effects of the jet are less pronounced.

The instantaneous interaction between the randomly oscillating jets and the cross flow is assessed using a proper orthogonal decomposition (POD), computed by singular value decomposition, for the set of 500 instantaneous flow field measurements from which the results in Figure 11 were computed. Subsequently, the flow fields are reconstructed using the 30 most energetic modes, representing 32% of the total fluctuating energy. Figure 12 shows reconstructions of two selected instantaneous realizations, consisting of in-plane velocity vectors with color contours of u_t, ω_t and u_r. The tangential velocity distributions vary between realizations I and II (Figures 12a and 12d, respectively) due to differences in the random instantaneous jet oscillation phases. The corresponding vorticity distributions are relatively chaotic and disorderly for realization I (Figure 12b) and better organized for realization II (Figure 12e). In realization I, the radial velocity (Figure 12c) is relatively uniform across the span, while realization II (Figure 12f) shows strong concentrations of radially-outward flow near $z/D = -0.1$ and radially-inward flow near $z/D = 0.09$ that are characteristic of interactions between the oscillating jets and the cross flow (cf. Figure 11).

To characterize the effect on the flow of an individual jet, the instantaneous direction of the jet at $z/D = 0$ for each reconstructed realization at $\theta = 116°$ is estimated by computing the angle β between the local surface tangent and the velocity vector at $z/D = 0$ and radial position h/D where local momentum is maximized (Figure 13a). The probability distribution function of β (Figure 13b) is symmetric about $\beta = 0$, indicating that the jet is not predominantly oriented toward either

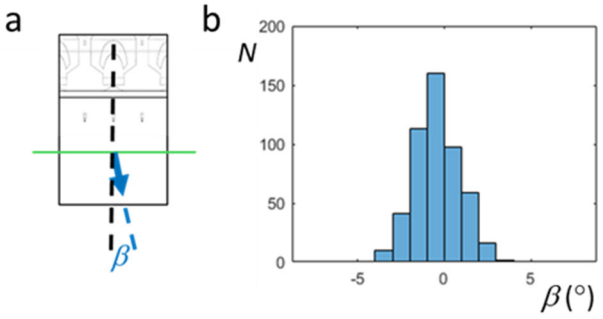

Figure 13. *(a) Velocity vector angle in boundary layer (β) downstream of central jet ($\alpha = 100°$, $z/D = 0$) at $\theta = 116°$. (b) Probability distribution function of β for $C_\mu^F = 3.1\%$.*

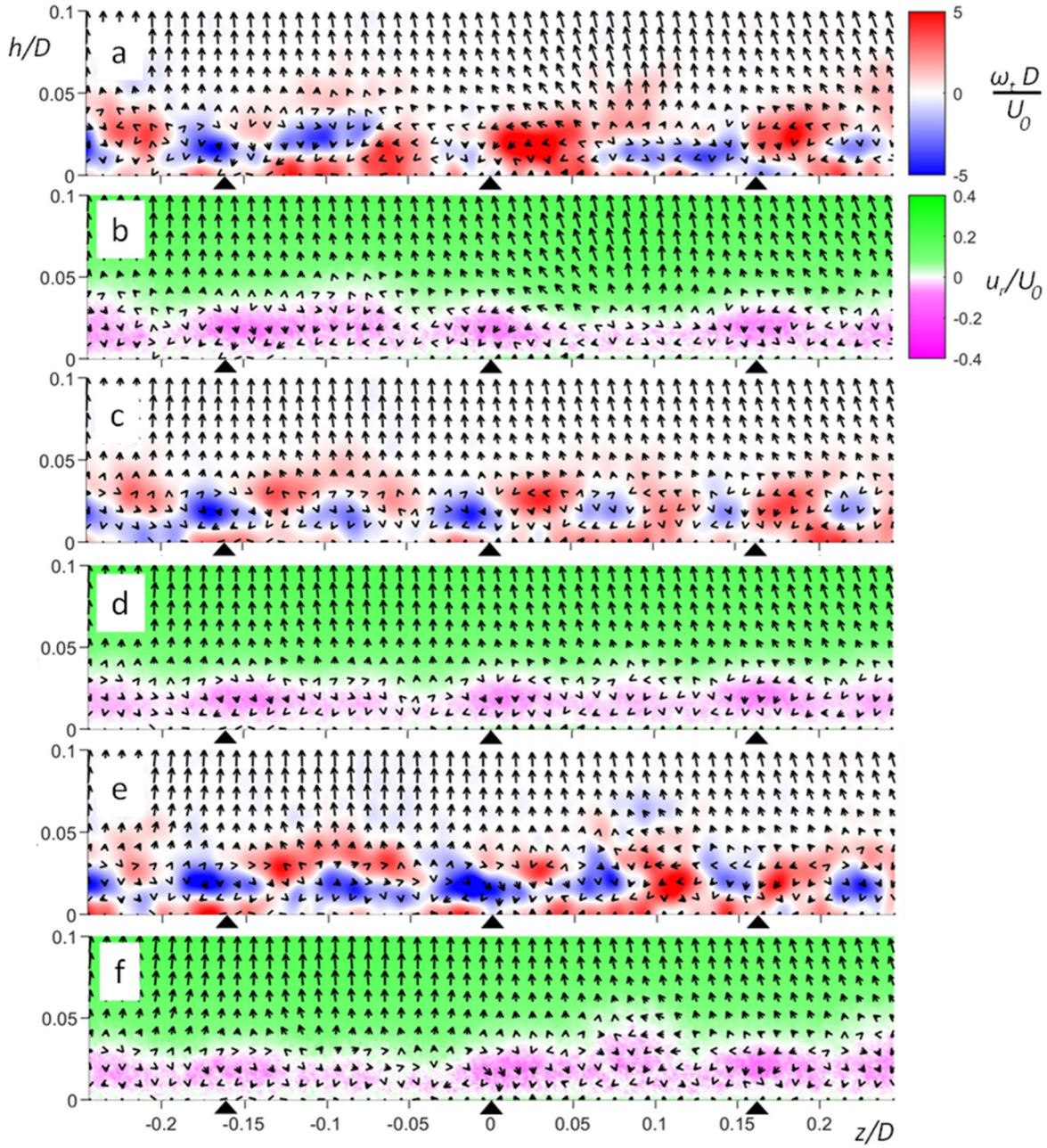

Figure 14. *Flow fields conditionally averaged in β from measurements in Figure 11: (a,b) -3° ≤ β < -2°, (c,d) -0.5° ≤ β < 0.5°, (e,f) 2° ≤ β < 3°. Color contours of (a,c,e) in-plane vorticity and (b,d,f) radial velocity. Triangles denote spanwise positions of jets.*

side. The reconstructions were then conditionally averaged according to β as indicated in Figure 14, where in-plane velocity vectors are shown along with color contours of ω_t and u_r. The conditional average for -3° ≤ β < -2° (Figures 14a and 14b), where the jet is oriented in the -z direction, is characterized by increased counterclockwise vorticity near $z/D = 0.03$. Correspondingly, the radial velocity is more radial-inward to the left of the jet, and more radial-outward to the right. By comparison, with the jet oriented nearly directly downstream (-0.5° ≤ β < 0.5°; Figures 14c and 14d) the vorticity and radial velocity distributions are relatively

symmetric about the jet centerline. With the jet oriented in the +z direction ($2° \leq \beta < 3°$; Figures 14e and 14f), a large concentration of clockwise vorticity is present near $z/D = -0.01$, and the resulting radial velocity distribution near the wall is opposite to when the jet is oriented in the $-z$ direction. These results suggest that as the jet oscillates, fluid transfer between the wall and the cross flow occurs at varying spanwise locations according to the phase of the jet oscillation. Outside of $-0.1 < z/D < 0.1$, both vorticity and radial velocity do not vary significantly with β (which is computed from the flow direction downstream of the center jet), indicating no significant coupling between oscillations of neighboring jets.

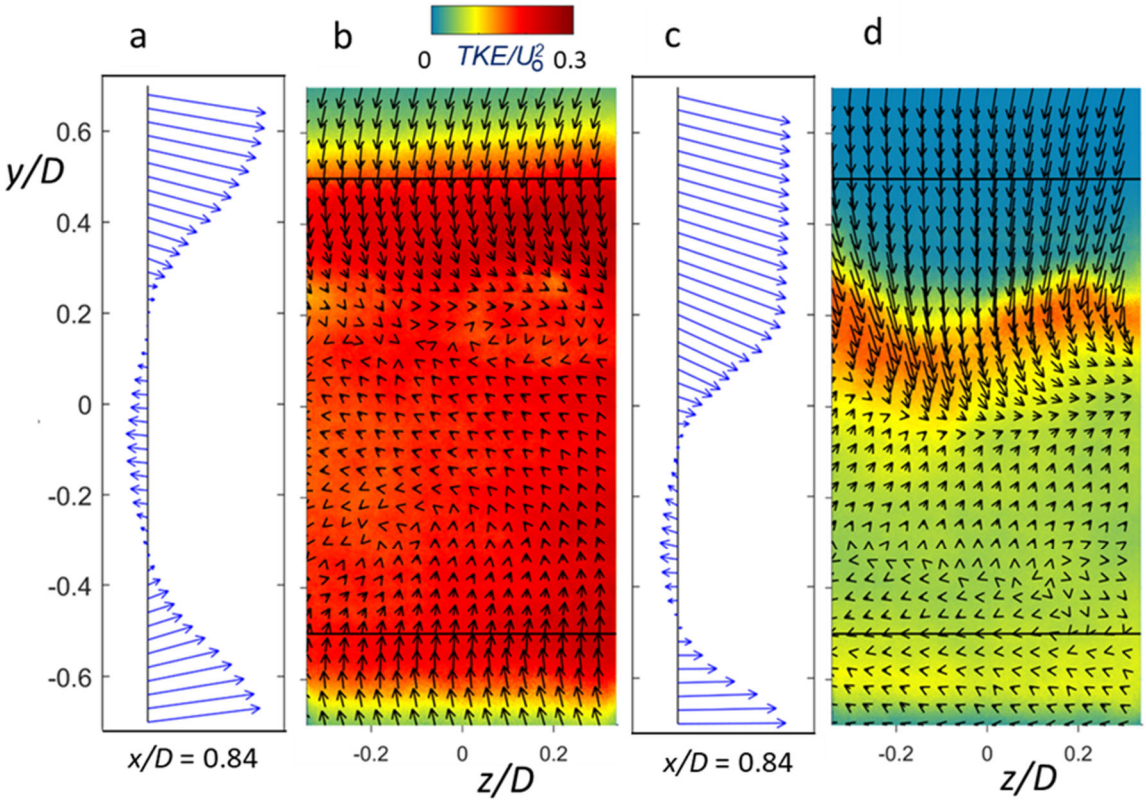

Figure 15. *Cross-stream velocity profile (z = 0; a,c) and streamwise-normal flow field (b,d) 0.84D downstream of cylinder center with color contours of turbulent kinetic energy and horizontal black lines denoting projection of cylinder. Jets at α = 100°; C_μ^F = 0 (a,b) and 0.031 (c, d).*

The effect of actuation on the near wake is assessed using stereo PIV measurements in a streamwise-normal plane 0.84D downstream of the model center. Cross-stream velocity profiles along the centerline of the model ($z = 0$; Figures 15a and 15c) indicate the cross-stream extent of the wake, the magnitude and direction of the upper and lower wakes, and the velocity deficit within the center of the wake. In the absence of actuation ($C_\mu^F = 0$; Figure 15a), the upper and lower wakes are nearly symmetrical, converge toward the model centerline, and have a speed greater than U_0 as the flow separates on the leeward side. Due to the presence of the recess containing the actuator orifice, the flow over the cylinder is not perfectly symmetrical between the upper and lower surfaces, as suggested by the slightly asymmetric velocity distribution in the central portion of the wake. With actuation at $\alpha = 100°$, i.e. on the upper surface ($C_\mu^F = 0.031$; Figure 15c), the flow over the upper surface is drawn toward the wall and directed downward (cf. Figure 9c), resulting in additional circulation and hence higher lift (cf. Figures 5-7), as well as a significant

reduction in the width of the wake. The wake on the lower surface is turned downward only slightly.

The spanwise variation of the wake is indicated with the time-averaged in-plane flow field, along with color contours of TKE. In the absence of actuation (Figure 15b) the wake is nearly uniform across the span due to the smooth cylinder surface lacking spanwise variation. As noted in connection with Figure 10f, because separation is not uniform across the span in the presence of actuation (C_μ^F = 0.031), some spanwise variation in the wake is present, particularly near the upper edge where the cross-stream velocity gradient is largest. Turbulent fluctuation is reduced substantially in the actuated wake (C_μ^F = 0.031; Figure 15d), potentially because the eddy shedding of the cylinder is diminished by the vectored flow or because larger turbulent structures within the wake dissipate due to the high-frequency actuation of the fluidically oscillating jets. In the presence of actuation, TKE is greatest within the areas of high velocity gradient, as expected for a free shear layer, and becomes diminished both in the center of the wake and in the free stream.

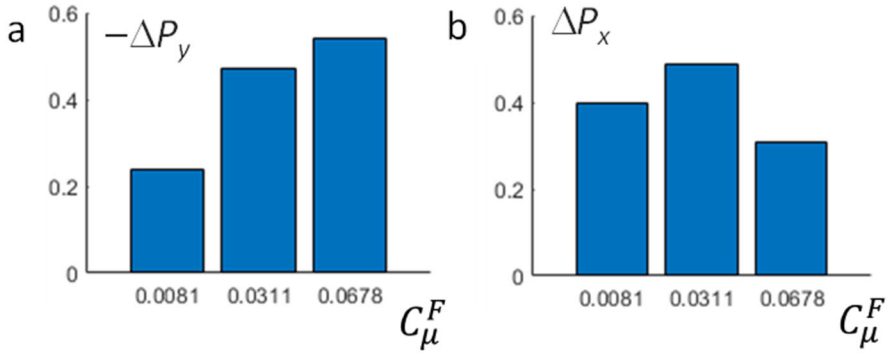

Figure 16. *Increment in (a) cross-stream and (b) streamwise momentum flux between C_μ^F = 3.1% and C_μ = 0 from measurements in Figures 15d and 15b, respectively.*

The increment due to actuation (C_μ^F = 0.008, 0.031 and 0.067) of the cross-stream and streamwise momentum fluxes through the near-wake PIV plane (cf. Figure 15) is shown in Figures 16a and 16b, respectively. As expected for increased lift, the cross-stream momentum flux becomes increasingly downward as C_μ^F is increased (Figure 16a), and the streamwise momentum flux also increases in the presence actuation (Figure 16b), indicating drag reduction, in agreement with aerodynamic load measurements (cf. Figure 7).

V. CONCLUSIONS

The present wind tunnel investigations explore the utility of segmented Coanda actuation on a circular cylinder model for generating streamwise and cross-stream loads using spanwise arrays of fluidically oscillating wall jets with specific emphasis on the interaction of the control jets with the cross flow and their effects on the near wake.

It is shown that the 3-D actuation using a spanwise array of 3-D fluidically-oscillating wall jets is effective in regulating the normal and streamwise aerodynamic loads in the absence and presence of surface trips. In the presence of surface-periodic tripping, the effect of the azimuthal jet position in the absence of actuation is significantly diminished and the overall cylinder drag is similar to the drag when the surface boundary layer is turbulent (the drag variation with the azimuthal position of the jets varies by 8% relative to the baseline, turbulent level). For a given actuation

level, the lift increases monotonically with α up to C_L = 1.5 at C_μ^F = 0.087 followed by a decrease towards the leeward side of the cylinder. In the absence of trips on a smooth cylinder, the baseline drag coefficient is similar to that in laminar separation, or about 1.2 when the actuator is on the leeward side and 0.97 when the actuator is on the windward side. Actuation leads to a remarkable reduction in drag down to the level of the periodically tripped cylinder. The rate of increase in lift with α is significantly higher for the smooth cylinder without trips than in the presence of surface trips, and the lift rises to as high as C_L = 2.5 at C_μ^F = 0.076. It is noteworthy that the lift generated by the fluidically oscillating jets at a given mass flow rate (same C_q) is typically significantly higher than the corresponding lift generated by 2-D jets.

Using conditional sampling based on POD of instantaneous PIV data, it is shown that the interaction of wall-tangential 3-D oscillating jets with the cross flow is characterized by formation of spanwise-shifting counter-rotating vorticity concentrations over the surface of the cylinder through which higher-momentum fluid is entrained from the cross flow toward the surface, leading to vectoring of the forced side of the near wake and increased lift. Since the jets oscillate across the span, the spanwise extent over which the cross-stream flow is entrained toward the surface is significantly wider than the spanwise extent of the jets. It is conjectured that the interactions between adjacent jets at random phases may lead to an efficient spanwise distribution of momentum transfer compared to steady jets. The present measurements also show that the unforced side of the near wake is not deflected relative to the cylinder, such that the width of the wake is greatly diminished, and that concentrations of TKE are significantly diminished due to small-scale high-frequency forcing from the oscillating jets.

REFERENCES

Berkooz, G., Holmes, P. and Lumley, J. L., "The Proper Orthogonal Decomposition in the Analysis of Turbulent Flows," *Annual Review of Fluid Mechanics*, Vol. 25, No. 1, pp. 539-575, January 1993. https://doi.org/10.1146/annurev.fl.25.010193.002543

Dionisio, F. A. and Nurick, A., "Investigation of a Circulation Controlled Cylinder using an Adaptive Wall Wind Tunnel," *J. Aircraft*, Vol. 38, No. 3, pp. 521-527, May 2001. https://doi.org/10.2514/2.2792

Dunham, J., "A Theory of Circulation Control by Slot-Blowing, Applied to a Circular Cylinder," *J. Fluid Mechanics,* Vol. 33, No. 3, pp. 495-514, September 1968. https://doi.org/10.1017/S0022112068001473

Englar, R. J., "Circulation Control Pneumatic Aerodynamics: Blown Force and Moment Augmentation and Modification; Past, Present and Future," AIAA 2000-2541, AIAA Fluids 2000 Meeting, Denver, CO, June 19-22, 2000. https://doi.org/10.2514/6.2000-2541

Englar R. J., "Overview of Circulation Control Pneumatic Aerodynamics: Blown Force and Moment Augmentation and Modification as Applied Primarily to Fixed-Wing Aircraft," *Applications of Circulation Control Technologies*, R. D. Joslin and G. S. Jones Eds, Progress In Astronautics and Aeronautics, Volume 214, 2006.

Ghee, T. A. and Leishman, J. G., "Unsteady Circulation Control Aerodynamics of a Circular Cylinder with Periodic Jet Blowing," *AIAA J.*, Vol. 30, No. 2, pp. 289-299, February 1992. https://doi.org/10.2514/3.10916

Hanvey, S., "NOTAR – No Tail Rotor (Circulation Control Tail Boom)," Presented in *Report to the Aerospace Profession – Proceedings of the 26th Symposium*, pp. 308-332, 1982.

Hoerner, S., *Fluid-Dynamic Drag: Practical Information on Aerodynamic Drag and Hydrodynamic Resistance*, Hoerner Fluid Dynamics: Bakersfield, CA, 1965.

Jones, G. and Englar, R., "Advances in Pneumatic-Controlled High-Lift Systems through Pulsed Blowing," AIAA 2003-3411, June 2003. https://doi.org/10.2514/6.2003-3411

Klemin, A., "The Problem of the Helicopter," *The Scientific Monthly*, Vol. 67, No. 2, pp. 127-130, August 1948. https://www.jstor.org/stable/22321

Launder, B. E. and Rodi, W., "The Turbulent Wall Jet – Measurements and Modeling," *Annual Review of Fluid Mechanics*, Vol. 15, pp. 429-459, January 1983. https://doi.org/10.1146/annurev.fl.15.010183.002241

Levinsky, E. S. and Yeh, T. T., "Analytical and Experimental Investigation of Circulation Control by Means of a Turbulent Coanda Jet," NASA CR-2114, September 1972. https://ntrs.nasa.gov/api/citations/19720023364/downloads/19720023364.pdf

Lockwood, V., "Lift Generation on a Circular Cylinder by Tangential Blowing from Surface Slots," NASA TN D-244, May 1960. http://catalog.hathitrust.org/api/volumes/oclc/73507654.html

Logan, A. and Kumar, K., "NOTAR Helicopter – A New Approach to Helicopters," Presented at Society of Allied Weight Engineers 45th annual conference, Williamsburg, Virginia, USA, May 1986. https://www.sawe.org/papers/1734

Loth, J. and Boasson, M., "Circulation Controlled STOL Wing Optimization," *Journal of Aircraft*, Vol. 21, No. 2, pp. 128-134, February 1984. https://doi.org/10.2514/3.48235

Luo, X., Zhang, C. and Wang, H., "Experimental Study of No Tail Rotor (NOTAR) Helicopter," Presented at ICAS 2000 Congress, Harrogate, UK, August 2000. https://www.icas.org/ICAS_ARCHIVE/ICAS2000/PAPERS/ICA0181.PDF

McDaniel, R., "Jet Thrust as a Counter-Torque Force for Single-Rotor, Shaft-Powered Helicopters," Ph.D. Dissertation, Georgia Institute of Technology, June 1961.

Neuendorf, R. and Wygnanski, I., "On a Turbulent Wall Jet Flowing over a Circular Cylinder," *J. Fluid Mechanics,* Vol. 381, pp. 1-25, February 1999. https://doi.org/10.1017/S0022112098003668

Neuendorf, R., Lourenco, L. and Wygnanski, I., "On Large Streamwise Structures in a Wall Jet Flowing over a Circular Cylinder," *Physics of Fluids*, Vol. 16, No. 7, pp. 2158-2169, July 2004. https://doi.org/10.1063/1.1703531

Newman, B. G., "The Deflexion of Plane Jets by Adjacent Boundaries – Coanda Effect," in *Boundary Layer and Flow Control: Its Principles and Applications, Volume 1*, Pergamon Press, edited by G. V. Lachmann, pp. 232-264, 1961.

Nichols, J. and Englar, R., "Advanced Circulation Control Wing System for Navy STOL Aircraft," AIAA 1980-1825, August 1980. https://doi.org/10.2514/6.1980-1825

Nurick, A., "Experimental Investigation of a Helicopter Circulation-Controlled Tail Boom," *J. Aircraft,* Vol. 38, No. 3, pp. 528-535, May 2001. https://doi.org/10.2514/2.2793

Oh, S. and Roberts, L., "Control of Separated Flow Past a Cylinder using Tangential Wall Jet Blowing," NASA CR-185918, July 1989. https://ntrs.nasa.gov/api/citations/19890019955/downloads/19890019955.pdf

Runge, W., Buysschaert, F., Hayez, J., Carlier, F., Antoine, H., Hendrick, P., Dimitriadis, G. and Degrez, G., "Numerical and Experimental Investigation of Slot-Blown Air over a Cylinder," *Progress in Flight Physics*, Vol. 7, pp. 229-244, June 2015. https://doi.org/10.1051/eucass/201507229

Sampatacos, E., Morger, K. and Logan, A., "NOTAR: The Viable Alternative to a Tail Rotor," AIAA 1983-2527, October 1983. https://doi.org/10.2514/6.1983-2527

Shih, W., Wang, C., Coles, D. and Roshko, A., "Experiments on Flow Past Rough Circular Cylinders at Large Reynolds Numbers," *Journal of Wind Engineering and Industrial Aerodynamics*, Vol. 49, No. 1-3, pp. 351-368, December 1993. https://doi.org/10.1016/0167-6105(93)90030-R

Sikorsky, I., "Technical Development of the VS-300 Helicopter during 1941," *Journal of the Aeronautical Sciences*, Vol. 9, No. 8, pp. 309-311, June 1942. https://doi.org/10.2514/8.10892

Sirovich, L., "Turbulence and the Dynamics of Coherent Structures Part I: Coherent Structures," *Quarterly of Applied Mathematics*, Vol. 45, No. 3, pp. 561-571, October 1987. https://doi.org/10.1090/qam/910462

Vukasinovic, B., Funk, R. and Glezer, A., "Circulation Control using Arrays of Discrete Fluidic Actuator Jets," AIAA 2023-1992, January 2023. https://doi.org/ 10.2514/6.2023-1992

Williams, J. and Cummings, R., "Experimental Investigation of a Circular Cylinder under the Effects of Tangential Slot Blowing," AIAA 1996-2435, June 1996. https://doi.org/10.2514/6.1996-2435

Zandieh, A. and Leishman, J. G., "Boundary Layer and Pressure Measurements on a Cylinder with Unsteady Circulation Control," *AIAA Journal*, Vol. 31, No. 10, pp. 1769-1776, October 1993. https://doi.org/10.2514/3.49107

Zdravkovich, M. M., "Conceptual Overview of Laminar and Turbulent Flows Past Smooth and Rough Circular Cylinders," *Journal of Wind Engineering and Industrial Aerodynamics*, Vol. 33, No. 1-2, pp. 53-62, March 1990. https://doi.org/10.1016/0167-6105(90)90020-D